



Journal of Applied and Computational Mechanics



Research Paper

The Effect of Delamination Between Layers in U-shaped Members Made of Functionally Graded Multilayered Viscoelastic Materials

Victor Rizov^{id}

Department of Technical Mechanics, University of Architecture, Civil Engineering and Geodesy, 1 Chr. Smirnensky blvd., Sofia, 1046, Bulgaria, Email: V_RIZOV_FHE@UACG.BG

Received February 01 2024; Revised April 16 2024; Accepted for publication May 15 2024.

Corresponding author: V. Rizov (V_RIZOV_FHE@UACG.BG)

© 2024 Published by Shahid Chamran University of Ahvaz

Abstract. This theoretical work deals with delamination in U-shaped load-carrying structural members. The latter represent multilayered functionally graded systems of non-linear viscoelastic behaviour. The right-hand vertical part of the structure under consideration is delaminated. The structure is clamped in the lower end of the left-hand vertical part. Besides, the structure is supported by a rotational spring which has non-linear elastic behaviour. The strain energy release rate is derived by using an approach that is based on analysis of equilibrium of the various components of the U-shaped structure. The solution derived is checked-up by applying the method of the integral J . The dependence of the strain energy release rate on different parameters is studied and presented in form of various graphs. Analysis of a U-shaped structural member with two rotational spring supports also is carried-out and the strain energy release rate obtained is compared with that in the U-shaped structure with one rotational spring support.

Keywords: U-shaped member, Multilayered load-carrying system, Functionally graded structure, Delamination, Equilibrium equation.

1. Introduction

It is now widely appreciated that using multilayered and functionally graded materials play an important role for improving the overall performance of various structures, mechanisms and devices in different sectors of modern engineering [1]. The basic idea of a multilayered system is to use the advantages of different materials by combining them in an integrated engineering structure consisting of layers made of materials with different properties [2, 3]. Therefore, at the time being, multilayered constructions are an attractive design for load-carrying structural members and components, having an efficient bending stiffness and relatively lesser weight compared to homogeneous structural materials.

Over the recent decades, a class of continuously inhomogeneous advanced composites known as functionally graded materials have been used in a broad range of engineering applications including for structural purposes in construction and automotive industries, aerospace, nuclear power plants, and many others [4-9]. As known, the concept for the functionally graded materials consists in the fact that their composition and macrostructure can be varied spatially in a structural member [10-15]. This concept enables manufacturing of highly efficient structures of tailored continuous distribution of material properties to meet diverse exploitation requirements [16-20].

One of the potential applications of multilayered functionally graded material systems is U-shaped structural members. The U-shaped members are important components in different structures in civil engineering and machinery construction. In view of the excellent properties of multilayered functionally graded material systems, the use of multilayered functionally graded U-shaped structural members seems to be a very good choice. However, together with their undisputable advantages, the multilayered materials and structural components have some drawbacks which slow up their wide acceptance in load-carrying structures including in the U-shaped structural members. One of the main reasons for uncertainty in applying multilayered materials is the delamination. As known, the delamination is a failure mechanism representing separation of layers that can have catastrophic consequences for the reliability and safety of the multilayered structure. Delamination usually causes sharp reduction of load-carrying ability of multilayered structural members and components, increases their deformability and has a negative influence of stability of these structures when they are subjected to compressive external loading. Durability of multilayered engineering structures is also significantly affected by their delamination behaviour. In the past, various models of layered load-carrying beam structures with delamination were proposed and specific aspects of their behaviours under different loading conditions were analyzed in detail and are well understood [21-25]. However, the investigations of layered beam structures with delaminations being performed to date mostly assume linear-elastic mechanical behaviour of the material. Besides, the layered beam structures with delaminations being investigated to date are mainly those of rectilinear geometry [21-25].



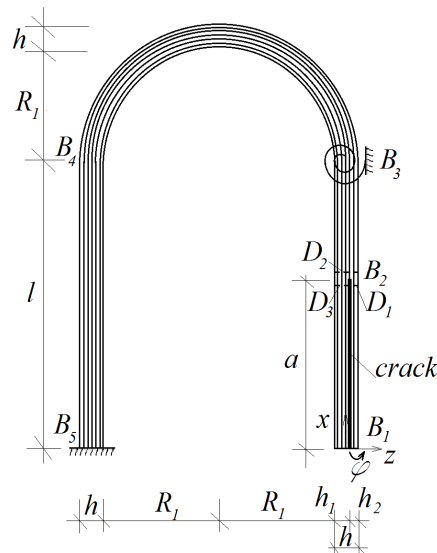


Fig. 1. Schema of the U-shaped structural member supported with a rotational spring in section, B_3 .

However, multilayered beam-like structures of non-rectilinear geometry occur frequently in up-to-date engineering. Obviously, analysis of delamination in such structures is of very significant importance for covering of their safety. Therefore, in this paper, a U-shaped load-carrying beam structural member with a delamination is analyzed theoretically. The member is made of multilayered functionally graded material with non-linear viscoelastic behaviour. Besides the clamping in the lower end of its left-hand vertical part, the member is supported also by a rotational spring support of non-linear elastic behaviour. Using of rotational springs for supporting of structures is analyzed in the research literature [26]. However, the analyses in [26, 27] deal with linear-elastic homogeneous beams of rectilinear geometry. Besides, the beams in [26, 27] do not host delamination. In this paper, the strain energy release rate (SERR) is derived and checked-up by utilizing of the integral J . The effects of broad spectra of parameters and factors on delamination in the U-shaped structure are investigated. The dependences of the SERR on these parameters and factors are presented in form of various graphs. A U-shaped structural member supported with two rotational spring supports of non-linear elastic behaviour is also analyzed in order to see what the effects of these supports on the delamination are. Some possible practical applications of the analysis developed here in the engineering design of U-shaped multilayered functionally graded structural members with considering delamination behaviour are specified in the conclusion section of the present paper.

2. Theoretical Analysis

Consider the load-carrying beam member bent into a U-shape as displayed in Fig. 1. The member is made of longitudinal layers (their number is n). The length of the vertical parts, B_1B_3 and B_4B_5 , is l (Fig. 1). b and h are the width and thickness of the member cross-section (the latter is a rectangle as displayed in Fig. 2).

The part, B_3B_4 , of the member is a semicircle whose internal radius is R_1 . The member is clamped in section, B_5 . Besides, the member is supported by a rotational spring in section, B_3 , as displayed in Fig. 1.

This rotational spring is non-linear elastic and its behaviour is presented by the following non-linear law:

$$M_{B3} = \rho \phi_{B3}^m, \tag{1}$$

where M_{B3} is the restoring couple in the spring, ρ is the spring stiffness, m is a constant, ϕ_{B3} is the angle of rotation of section, B_3 , of the member. A delamination of length, a , splits part, B_1B_2 , of the member (Fig. 1). The thicknesses of the left-hand and right-hand delamination arms are h_1 and h_2 , respectively. Eq. (1) is a power law widely applied for non-linear elastic springs [28].

The lower end of the right-hand delamination arm (this with thickness, h_2) is under angle of rotation, ϕ , that varies with time, t . This variation is described by the following law:

$$\phi = \theta \ln(1 + \lambda t), \tag{2}$$

where θ and λ are parameters controlling the variation. The angle rotation, ϕ is in-plane. The idea of using Eq. (2) is to show, in principle, how U-shaped beams with delamination can be analyzed when the angle of rotation changes smoothly with time.

The layers of the member have non-linear viscoelastic behaviour. Formula (3) represents the non-linear stress-strain-time relationship describing the behaviour of the i -th layer of the member [29]:

$$\sigma_i(\varepsilon, t) = \psi_{1i}(\varepsilon) \psi_{2i}(t), \tag{3}$$

where

$$\psi_{1i} = \frac{L_i \varepsilon}{\sqrt{1 + f_i \varepsilon^2}}, \tag{4}$$

$$\psi_{2i} = \frac{1}{1 + \beta_i t^{\alpha_i}}, \tag{5}$$

$$i = 1, 2, \dots, n. \tag{6}$$



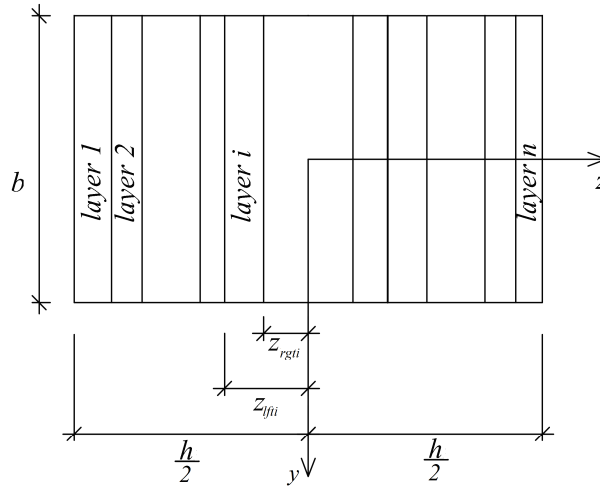


Fig. 2. Cross-section of the U-shaped structural member.

In formulas (3), (4) and (5), σ_i is the stress, ε is the strain, L_i , f_i , β_i and δ_i are material properties. Formula (3) indicates that the stress-strain-time relationship represents a product of two functions, ψ_{1i} and ψ_{2i} , where ψ_{1i} is function of strains, ψ_{2i} is function of time only. In fact, ψ_{1i} describes the stress-strain diagram of the material since at $t=0$ the value of ψ_{2i} is unit [29]. The time-dependent behaviour is described by function, ψ_{2i} [29].

The layers of the member are functionally graded along the thickness. Therefore, the material properties vary continuously along the layer thickness. These variations are described by the following laws:

$$L_i = L_{lfti} + \frac{L_{rgti} - L_{lfti}}{(z_{rgti} - z_{lfti})^{q_i}} (z - z_{lfti})^{q_i}, \quad (7)$$

$$f_i = f_{lfti} + \frac{f_{rgti} - f_{lfti}}{(z_{rgti} - z_{lfti})^{g_i}} (z - z_{lfti})^{g_i}, \quad (8)$$

$$\beta_i = \beta_{lfti} + \frac{\beta_{rgti} - \beta_{lfti}}{(z_{rgti} - z_{lfti})^{w_i}} (z - z_{lfti})^{w_i}, \quad (9)$$

$$\delta_i = \delta_{lfti} + \frac{\delta_{rgti} - \delta_{lfti}}{(z_{rgti} - z_{lfti})^{r_i}} (z - z_{lfti})^{r_i}, \quad (10)$$

$$z_{lfti} \leq z \leq z_{rgti}, \quad (11)$$

$$i = 1, 2, \dots, n. \quad (12)$$

In formulas (7) – (10), q_i , g_i , w_i and r_i are properties controlling the variations, the subscripts, $lfti$ and $rgti$, refer to the left-hand and right-hand surfaces of the i -th layer, respectively. Thus, z_{lfti} and z_{rgti} are the coordinates of these surfaces, z is the centric axis of the cross-section as displayed in Fig. 2. L_{lfti} , f_{lfti} , β_{lfti} and δ_{lfti} are the values of L_i , f_i , β_i and δ_i on the left-hand surface, P_{rgti} , f_{rgti} , β_{rgti} and δ_{rgti} are the values of L_i , f_i , β_i and δ_i on the right-hand surface of the layer.

As known, the SERR is one of the most important quantities analyzed in fracture mechanics. Utilizing the approach from [30], we derive formula (13) for the SERR, G , in the U-shaped member in Fig. 1:

$$G = \left(\sum_{i=1}^{i=n} \int_{z_{lfti}}^{z_{rgti}} u_{0B1B2i}^* dz_1 - \sum_{i=1}^{i=n} \int_{z_{lfti}}^{z_{rgti}} u_{0B2B3i}^* dz_2 \right), \quad (13)$$

where n_i is the number of layers in the right-hand delamination arm, u_{0B1B2i}^* and u_{0B2B3i}^* are the complementary strain energy densities in an arbitrary layer in the right-hand delamination arm and the intact part of the structural member ahead of the delamination, respectively, z_1 and z_2 are the centric axes of the cross-sections of the right-hand delamination arm and the intact part of the structural member ahead of the delamination. It should be specified that formula (13) is composed with taking into account the fact that the complementary strain energy in the left-hand delamination arm (this with thickness, h_1) is zero because this delamination arm is not loaded since the angle of rotation, ϕ , of the right-hand delamination arm is directed anticlockwise (Fig. 1).

Formula (14) is applied to obtain the complementary strain energy density in an arbitrary layer in the right-hand delamination arm, i.e.,

$$u_{0B1B2i}^* = \sigma_{B1B2i} \varepsilon_{B1B2i} - \int_0^{\varepsilon_{B1B2i}} \sigma_{B1B2i} d\varepsilon_{B1B2i}, \quad (14)$$



where the stress, $\sigma_{B_1B_2i}$, in the layer is found by using formula (3). Formula (14) is applied also to obtain $u'_{0B_2B_3i}$ (for this purpose, $\varepsilon_{B_1B_2}$ is replaced with the strain, $\varepsilon_{B_2B_3}$, in the intact part, B_2B_3 , of the structural member).

Formula (15) describes the variation of the strain along the thickness of the right-hand delamination arm:

$$\varepsilon_{B_1B_2} = \kappa_1(z_1 - z_{1n}), \tag{15}$$

where

$$-\frac{h_2}{2} \leq z_1 \leq \frac{h_2}{2}. \tag{16}$$

In formula (15), κ_1 is the curvature, z_{1n} is the coordinate of the neutral axis (formula (15) takes into account the fact that the neutral axis shifts from the cross-section centre because the member is inhomogeneous along the thickness).

Formula (17) is used for presenting the variation of the strain along the thickness in the intact part, B_2B_3 , of the structural member:

$$\varepsilon_{B_2B_3} = \kappa_2(z_2 - z_{2n}), \tag{17}$$

where

$$-\frac{h}{2} \leq z_2 \leq \frac{h}{2}. \tag{18}$$

Here, κ_2 and z_{2n} are the curvature and coordinate of the neutral axis, respectively.

The approach for determining the curvatures and the coordinates of the neutral axes developed in the present study uses the fact that the law for variation of the angle of rotation of the lower end of the right-hand delamination arm with time is known (refer to formula (2)). Therefore, first, ϕ is expressed by applying the integrals of Maxwell-Mohr:

$$\phi = \kappa_1 a + \kappa_2(l - a) + \kappa_3 l_{B_3B_4} + \kappa_4 l, \tag{19}$$

where κ_3 is the change of curvature in the curvilinear part, B_3B_4 , of the member, κ_4 is the curvature in part, B_4B_5 , of the member. The length of the curvilinear part, $l_{B_3B_4}$, that is involved in (19) is found by using formula (20), i.e.,

$$l_{B_3B_4} = \pi \left(R_1 + \frac{h}{2} \right). \tag{20}$$

Four equations are composed by using the fact that the axial forces, $N_{B_1B_2}$, $N_{B_2B_3}$, $N_{B_3B_4}$ and $N_{B_4B_5}$, in the four parts, B_1B_2 , B_2B_3 , B_3B_4 and B_4B_5 , of the U-shaped structural member are zero, i.e.,

$$N_{B_1B_2} = b \sum_{i=1}^{i=n_1} \int_{z_{1ft}}^{z_{1rgt}} \sigma_{B_1B_2i} dz_1 = 0, \tag{21}$$

$$N_{B_2B_3} = b \sum_{i=1}^{i=n} \int_{z_{2ft}}^{z_{2rgt}} \sigma_{B_2B_3i} dz_2 = 0, \tag{22}$$

$$N_{B_3B_4} = b \sum_{i=1}^{i=n} \int_{z_{3ft}}^{z_{3rgt}} \sigma_{B_3B_4i} dz_3 = 0, \tag{23}$$

$$N_{B_4B_5} = b \sum_{i=1}^{i=n} \int_{z_{4ft}}^{z_{4rgt}} \sigma_{B_4B_5i} dz_4 = 0, \tag{24}$$

where the stresses, $\sigma_{B_2B_3i}$, $\sigma_{B_3B_4i}$ and $\sigma_{B_4B_5i}$, in layers of parts, B_2B_3 , B_3B_4 and B_4B_5 , of the structural member are determined by replacing of ε with $\varepsilon_{B_2B_3}$, $\varepsilon_{B_3B_4}$ and $\varepsilon_{B_4B_5}$ in the law (3). Formulas (25) and (26) are used for describing the distributions of strains, $\varepsilon_{B_3B_4}$ and $\varepsilon_{B_4B_5}$, along the thickness of parts, B_3B_4 and B_4B_5 , respectively:

$$\varepsilon_{B_3B_4} = \kappa_3(z_3 - z_{3n}), \tag{25}$$

$$\varepsilon_{B_4B_5} = \kappa_4(z_4 - z_{4n}), \tag{26}$$

where z_{3n} and z_{4n} are the coordinates of the neutral axes in these parts of the member.

Three equations are composed by considering the equilibrium of sections, B_2 , B_3 and B_4 , of the member (Fig. 1), i.e.,

$$b \sum_{i=1}^{i=n_1} \int_{z_{1ft}}^{z_{1rgt}} \sigma_{B_1B_2i} z_1 dz_1 = b \sum_{i=1}^{i=n} \int_{z_{2ft}}^{z_{2rgt}} \sigma_{B_2B_3i} z_2 dz_2 = 0, \tag{27}$$

$$b \sum_{i=1}^{i=n} \int_{z_{2ft}}^{z_{2rgt}} \sigma_{B_2B_3i} z_2 dz_2 - b \sum_{i=1}^{i=n} \int_{z_{3ft}}^{z_{3rgt}} \sigma_{B_3B_4i} z_3 dz_3 = M_{B_3}, \tag{28}$$

$$b \sum_{i=1}^{i=n} \int_{z_{3ft}}^{z_{3rgt}} \sigma_{B_3B_4i} z_3 dz_3 = b \sum_{i=1}^{i=n} \int_{z_{4ft}}^{z_{4rgt}} \sigma_{B_4B_5i} z_4 dz_4 = 0, \tag{29}$$



where the restoring couple, M_{B_3} , in the rotational spring in section, B_3 , is found by applying formula (1). The angle of rotation, ϕ_{B_3} , that is involved in (1) is derived by the integrals of Maxwell-Mohr, i.e.,

$$\phi_{B_3} = \kappa_3 l_{B_3B_4} + \kappa_4 l. \quad (30)$$

Equations (19), (21)-(24), (27), (29) and (30) are used to determine the curvatures, κ_1 , κ_2 , κ_3 and κ_4 , the coordinates of the neutral axes, z_{1n} , z_{2n} , z_{3n} and z_{4n} , by the MatLab. Then the SERR is derived by applying formula (13). The integrals in (13) are solved by the MatLab.

The method of the J -integral is applied in order to perform a check-up of the SERR in the U-shaped member displayed in Fig. 1 [31]. For this purpose, the integration contour, $D_1 D_2 D_3$, is used (Fig. 1). This integration contour has three parts, D_1 , D_2 and D_3 , as displayed in Fig. 1. Since the left-hand delamination arm is not loaded, the value of the J -integral in part, D_3 , of the contour is zero. Therefore, the solution of the J -integral is:

$$J = J_{D_1} + J_{D_2}, \quad (31)$$

where J_{D_1} and J_{D_2} are the components in the contour parts, D_1 and D_2 , respectively.

Formula (32) is applied for obtaining of J_{D_1} , i.e.,

$$J_{D_1} = \sum_{i=1}^{i=n_1} \int_{z_{fui}}^{z_{1rgi}} \left[u_{0B_1B_2i} \cos \alpha - \left(p_{xi} \frac{\partial u}{\partial X} + p_{zi} \frac{\partial v}{\partial X} \right) \right] ds, \quad (32)$$

where $u_{0B_1B_2i}$ is the strain energy density in the i -th layer in the right-hand delamination arm. This strain energy density is found by applying formula (33):

$$u_{0B_1B_2i} = \int_0^{\varepsilon_{B_1B_2}} \sigma_{B_1B_2i} d\varepsilon_{B_1B_2}. \quad (33)$$

Formulas (34)–(38) are used for determining of other quantities involved in expression (32):

$$\cos \alpha = -1, \quad (34)$$

$$p_{xi} = -\sigma_{B_1B_2i}, \quad (35)$$

$$p_{zi} = 0, \quad (36)$$

$$\frac{\partial u}{\partial X} = \varepsilon_{B_1B_2}, \quad (37)$$

$$ds = dz_1, \quad (38)$$

where $\sigma_{B_1B_2i}$ and $\varepsilon_{B_1B_2}$ are obtained by applying formulas (3) and (15), respectively.

The component, J_{D_2} , is derived by using formula (39), i.e.,

$$J_{D_2} = \sum_{i=1}^{i=n} \int_{z_{fui}}^{z_{2rgi}} \left[u_{0B_2B_3i} \cos \alpha - \left(p_{xi} \frac{\partial u}{\partial X} + p_{zi} \frac{\partial v}{\partial X} \right) \right] ds. \quad (39)$$

Here, the strain energy density, $u_{0B_2B_3i}$, is found by formula (40):

$$u_{0B_2B_3i} = \int_0^{\varepsilon_{B_2B_3}} \sigma_{B_2B_3i} d\varepsilon_{B_2B_3}. \quad (40)$$

The rest of the quantities in Eq. (39) are obtained by using the following formulas:

$$\cos \alpha = 1, \quad (41)$$

$$p_{xi} = \sigma_{B_2B_3i}, \quad (42)$$

$$p_{zi} = 0, \quad (43)$$

$$\frac{\partial u}{\partial X} = \varepsilon_{B_2B_3}, \quad (44)$$

$$ds = -dz_1. \quad (45)$$

After substituting of (33) and (39) in formula (31), the integrals are solved by the MatLab. The results yielded by (31) match the SERR found by using formula (13) which is a check-up of the current analysis. Mathematical transformations proving that the method of the integral J yields results which coincide with formula (13) are shown too. These transformations are as follows. Eqs. (33) to (38) are plugged in Eq. (32), i.e.,



$$J_{D1} = \sum_{i=1}^{i=n_1} \int_{z_{1,fin}}^{z_{1,rgt}} \left[- \int_0^{c_{B1B2}} \sigma_{0B1B2i} d\varepsilon_{B1B2} + \sigma_{B1B2i} \varepsilon_{B1B2} \right] dz_1. \tag{46}$$

Using (14), one can reduce (46) to:

$$J_{D1} = \sum_{i=1}^{i=n_1} \int_{z_{1,fin}}^{z_{1,rgt}} u_{0B1B2i}^* dz_1. \tag{47}$$

Then, using Eqs. (40) to (45), Eq. (39) reduces to:

$$J_{D2} = - \sum_{i=1}^{i=n} \int_{z_{2,fin}}^{z_{2,rgt}} u_{0B2B3i}^* dz_2. \tag{48}$$

Now, Eq. (31) becomes:

$$J = \sum_{i=1}^{i=n_1} \int_{z_{1,fin}}^{z_{1,rgt}} u_{0B1B2i}^* dz_1 - \sum_{i=1}^{i=n} \int_{z_{2,fin}}^{z_{2,rgt}} u_{0B2B3i}^* dz_2 \tag{49}$$

that coincides with Eq. (13).

3. Numerical Results

In this section of the paper, numerical results obtained by applying the solution of the SERR (13) are presented.

The following data are used when deriving the numerical results: $b = 0,004$ m, $h = 0,005$ m, $l = 0.100$ m, $n = 5$, $n_1 = 2$, $R_1 = 0.400$ m, $\theta = 0.02$ rad, $\lambda = 10^{-6}$ and $\rho = 600$ Nm. The numerical results presented here reveal what are the effects of variation of different factors on the SERR (the latter is normalized as $G / (L_{yfl} b)$).

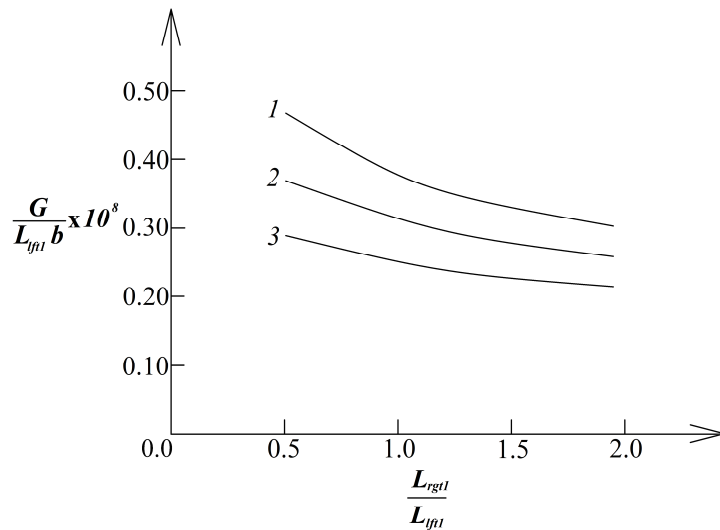


Fig. 3. The normalized SERR versus L_{rgt1} / L_{yfl} ratio for $n_1 = 2$ (curve 1), $n_1 = 3$ (curve 2) and $n_1 = 4$ (curve 3).

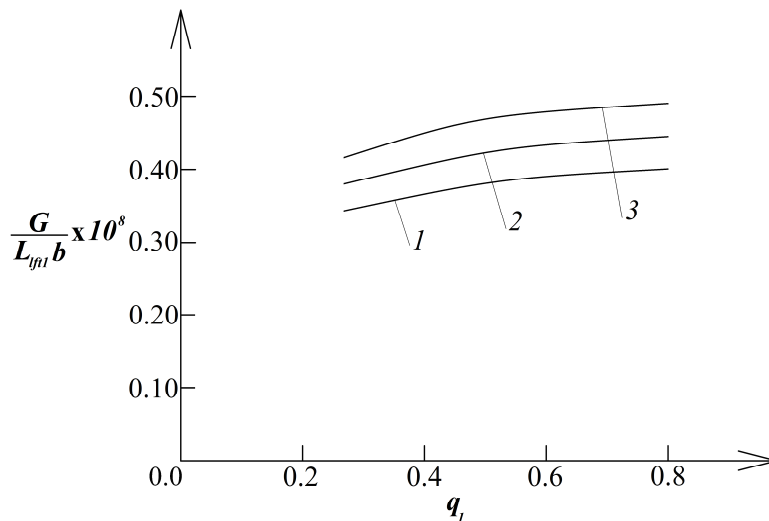


Fig. 4. The normalized SERR versus q_1 for $a / l = 0.4$ (curve 1), $a / l = 0.6$ (curve 2) and $a / l = 0.8$ (curve 3).



The effect of variation of L_{rgt1} / L_{lft1} ratio on the normalized SERR is illustrated by the curves plotted in Fig. 3.

The effect of the number of layers in the right-hand delamination arm is also considered. For this purpose, the normalized SERR is plotted against L_{rgt1} / L_{lft1} ratio for $n_1 = 2$, $n_1 = 3$ and $n_1 = 4$ in Fig. 3. The curves in Fig. 3 show significant dependence of the normalized SERR on both factors (L_{rgt1} / L_{lft1} ratio and the number of layers in the right-hand delamination arm).

This dependence is characterised by a strong reduction of the normalized SERR with rise of L_{rgt1} / L_{lft1} ratio and the number of layers in the right-hand delamination arm (Fig. 3).

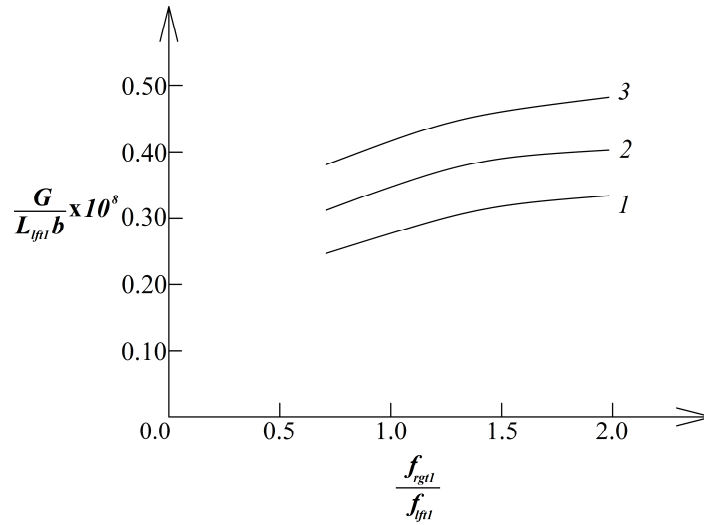


Fig. 5. The normalized SERR versus f_{rgt1} / f_{lft1} ratio for $l / h = 10$ (curve 1), $l / h = 15$ (curve 2) and $l / h = 20$ (curve 3).

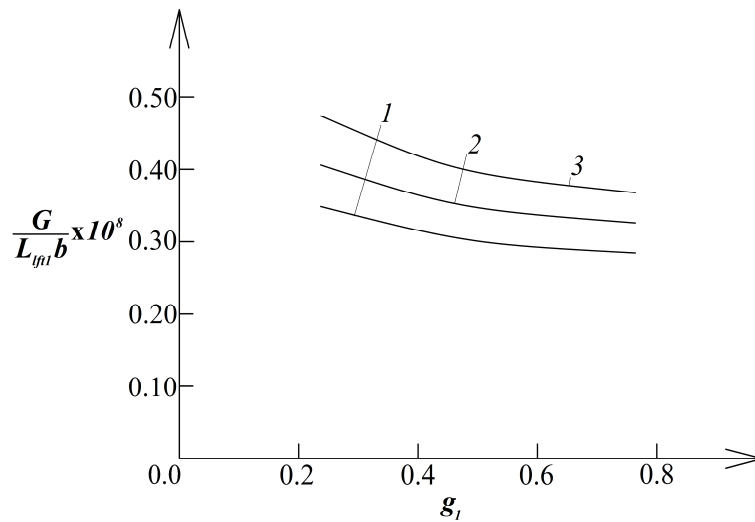


Fig. 6. The normalized SERR versus g_1 for $R_1 / l = 0.3$ (curve 1), $R_1 / l = 0.5$ (curve 2) and $R_1 / l = 0.7$ (curve 3).

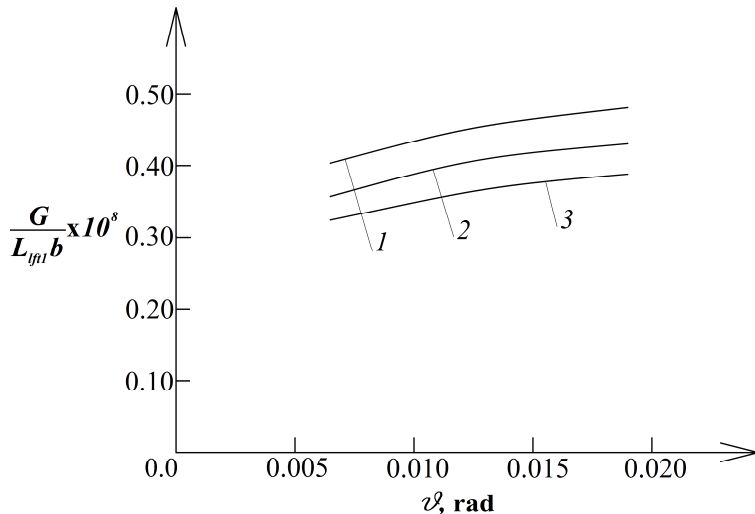


Fig. 7. The normalized SERR versus θ for $h / b = 1.3$ (curve 1), $h / b = 1.5$ (curve 2) and $h / b = 1.7$ (curve 3).



The explanation for the normalized SERR reduction with rise of L_{right1} / L_{left1} ratio consists in the growth of the stiffness of the U-shaped member. The reduction of the normalized SERR with increase on n_1 that can be observed in Fig. 3 is induced by the growth of right-hand delamination arm stiffness (remember that the left-hand delamination arm is not loaded).

Figure 4 displays the effect of the variation of a/l ratio on the dependence of the normalized SERR on the value of the parameter, q_1 . The curves plotted in Fig. 4 reveal a continuous growth of the normalized SERR with rise of q_1 for each of the considered a/l ratios. Besides, it is seen in Fig. 4 that the normalized SERR grows with rise of a/l ratio (the explanation of this fact is found in increase of deformability of the U-shaped structural member with increase of the delamination length).

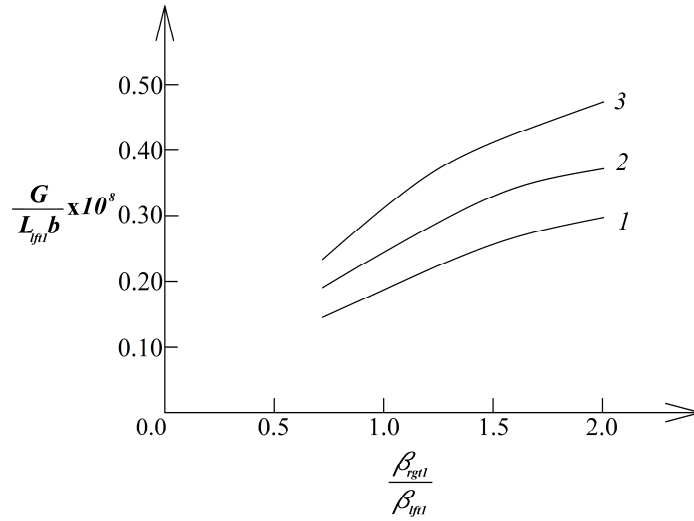


Fig. 8. The normalized SERR versus $\beta_{right1} / \beta_{left1}$ ratio for $\lambda = 1 \times 10^{-6}$ (curve 1), $\lambda = 3 \times 10^{-6}$ (curve 2) and $\lambda = 5 \times 10^{-6}$ (curve 3).

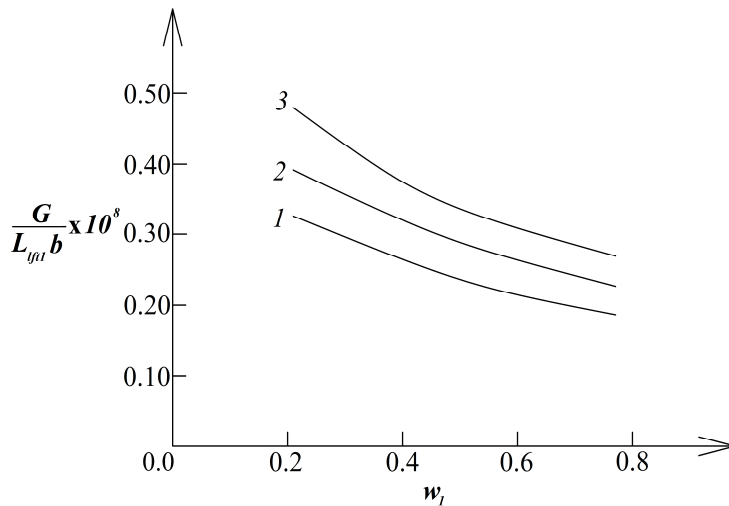


Fig. 9. The normalized SERR versus w_1 for $\delta_{right1} / \delta_{left1} = 0.5$ (curve 1), $\delta_{right1} / \delta_{left1} = 1.0$ (curve 2) and $\delta_{right1} / \delta_{left1} = 2.0$ (curve 3).

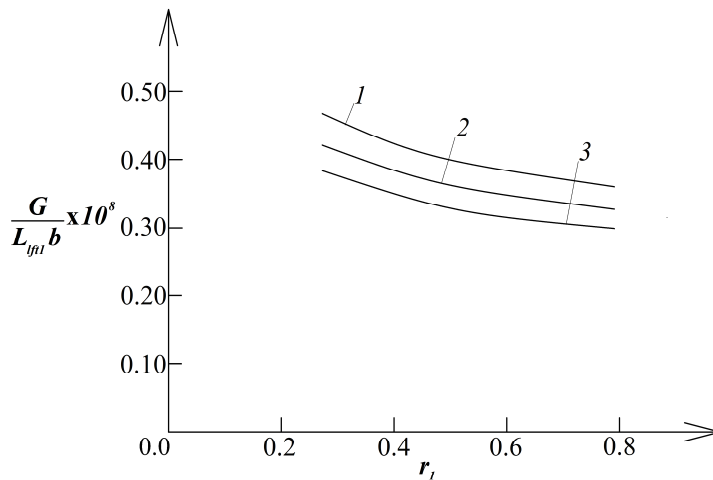


Fig. 10. The normalized SERR versus r_1 for $n = 3$ (curve 1), $n = 4$ (curve 2) and $n = 5$ (curve 3).



The dependence of the normalized SERR on f_{rgt1} / f_{jft1} ratio is illustrated in Fig. 5 for three l/h ratios. Here it is seen that rise of f_{rgt1} / f_{jft1} ratio induces rise of the normalized SERR (Fig. 5). Another feature that is expected is the rise of the normalized SERR with rise of l/h ratio (Fig. 5).

Figure 6 indicates the variation of the normalized SERR with respect to the parameter, g_1 . This variation is shown for three R_1/l ratios (Fig. 6). As displayed in these plots, the normalized SERR continuously reduces when g_1 grows (Fig. 6). The rise of the normalized SERR with rise of R_1/l ratio is related to increased deformability of the U-shaped structural member. The influence of h/b ratio on the dependence of the normalized SERR on the parameter, θ , is also an important consideration when analyzing delamination in the U-shaped structural member under angle of rotation varying with time according to law (2).

This influence is illustrated in Fig. 7, where the dependence of the normalized SERR on θ is plotted for three h/b ratios. The rise of the normalized SERR with rise of the value of θ is due to the growth of the angle of rotation of the lower end of the right-hand delamination arm. The reduction of the normalized SERR with growth of h/b ratio is generated by the increase of the stiffness of the U-shaped structural member (Fig. 7).

Displayed in Fig. 8 is the dependence of the normalized SERR on $\beta_{rgt1} / \beta_{jft1}$ ratio corresponding to three values of the parameter, λ . The rise of the normalized SERR when the parameter, λ , rises is attributed to increase of the angle of rotation, ϕ .

The variation of the normalized SERR due to the parameter, w_1 , and to $\delta_{rgt1} / \delta_{jft1}$ ratio is displayed in Fig. 9. The plots in Fig. 9 show reduction of the normalized SERR with rise of w_1 . An opposite trend, i.e., growth of the normalized SERR can be observed when $\delta_{rgt1} / \delta_{jft1}$ ratio rises (Fig. 9).

The effects of the values of the parameters, r_1 and n , on the normalized SERR are also analyzed and the corresponding plots are displayed in Fig. 10. The reduction of the normalized SERR when the number of layers, n , rises is explained by growth of the U-shaped structural member stiffness.

The influence of the restoring couple in the spring in section, B_3 , of the U-shaped structural member is considered too. For this purpose, the dependence of the normalized SERR on the parameter, m , is studied for three values of the parameter, ρ . The results of this study are illustrated by the plots displayed in Fig. 11. These plots show a growth of the normalized SERR when m rises. The growth of ρ generates reduction of the normalized SERR (Fig. 11).

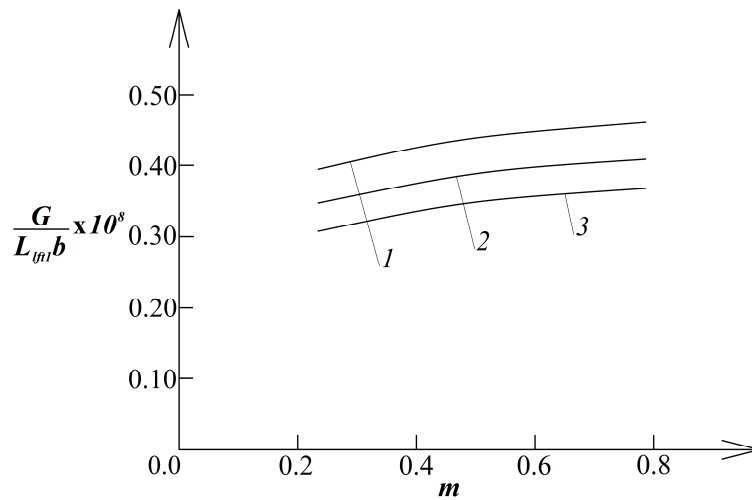


Fig. 11. The normalized SERR versus m for $\rho = 600$ Nm, (curve 1), $\rho = 900$ Nm (curve 2) and $\rho = 1200$ Nm (curve 3).

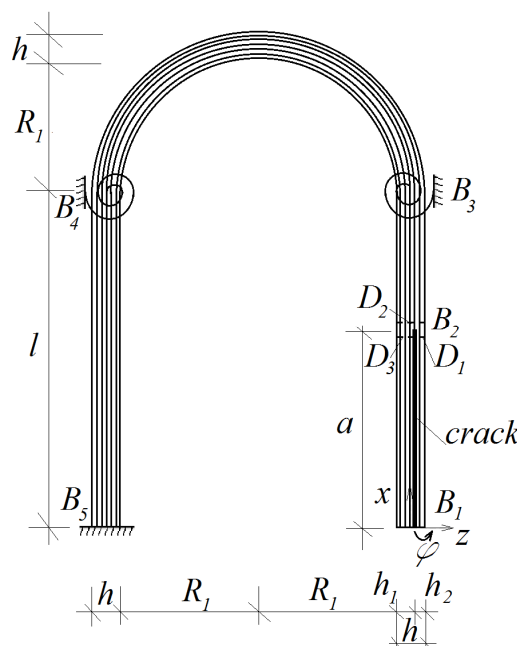


Fig. 12. Schema of the U-shaped structural member supported with rotational springs in sections, B_3 , and B_4 .



The analysis developed in section 2 of the present paper is applicable also when the U-shaped structural member under consideration is supported by more than one rotational spring. For instance, the U-shaped structural member displayed in Fig. 12 is supported by two rotational springs (one in section, B_3 , and another in section, B_1). Both rotational springs are non-linear elastic. The purpose of using rotational springs in different sections of the U-shaped beam is to impose unwanted constrains and to evaluate the effect of the positions of these constrains. The relation between the restoring couple, M_{B_4} , in the rotational spring in section, B_4 , of the U-shaped structural member and the angle of rotation, ϕ_{B_4} , of this section is presented by the non-linear law (46), i.e.,

$$M_{B_4} = \nu \phi_{B_4}^\omega, \tag{46}$$

where ν is the spring stiffness, ω is a constant. The behaviour of the rotational spring in section, B_3 , obeys law (1).

Section, B_5 , of the U-shaped structural member is clamped as displayed in Fig. 12. Part, B_1B_2 , of the structure is delaminated by a delamination of length, a , as shown in Fig. 12.

The angle of rotation of the lower end of the right-hand delamination arm (Fig. 12) varies with time according to formula (2). The variation of the material properties in the i -th layer obeys laws (7) to (10).

For the U-shaped structural member in Fig. 12, Eqs. (19), (21)-(24), (27), (29) and (30) can be used to determine the curvatures and the coordinates of the neutral axes. For this purpose, Eq. (29) has to be replaced by the following equilibrium equation:

$$b \sum_{i=1}^{i=n} \int_{z_{3jft}}^{z_{3rgt}} \sigma_{B3B4i} z_3 dz_3 - b \sum_{i=1}^{i=n} \int_{z_{4jft}}^{z_{4rgt}} \sigma_{B4B5i} z_4 dz_4 = M_{B_4}, \tag{47}$$

where M_{B_4} is found by using formula (46).

The strain energy release rate in Fig. 12 is obtained by applying formula (13). The method of the integral, J , is used for check-up of the strain energy release rate.

Displayed in Fig. 13 is the effect of the variation of ν / ρ ratio on the normalized SERR in the U-shaped structural member supported with two rotational springs. The normalized SERR for three L_{jft2} / L_{jft1} ratios, namely $L_{jft2} / L_{jft1} = 0.5$, $L_{jft2} / L_{jft1} = 1.0$ and $L_{jft2} / L_{jft1} = 2.0$, is obtained and shown in Fig. 13. The reduction of the normalized SERR with rise of ν / ρ and L_{jft2} / L_{jft1} ratios that can be observed in Fig. 13 is caused by the fact that the U-shaped structural member becomes stiffer.

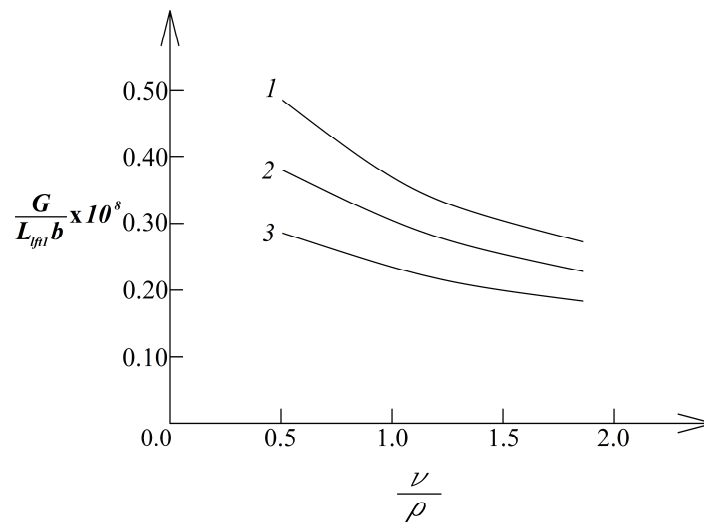


Fig. 13. The normalized SERR versus ν / ρ ratio for $L_{jft2} / L_{jft1} = 0.5$ (curve 1), $L_{jft2} / L_{jft1} = 1.0$ (curve 2) and $L_{jft2} / L_{jft1} = 2.0$ (curve 3).

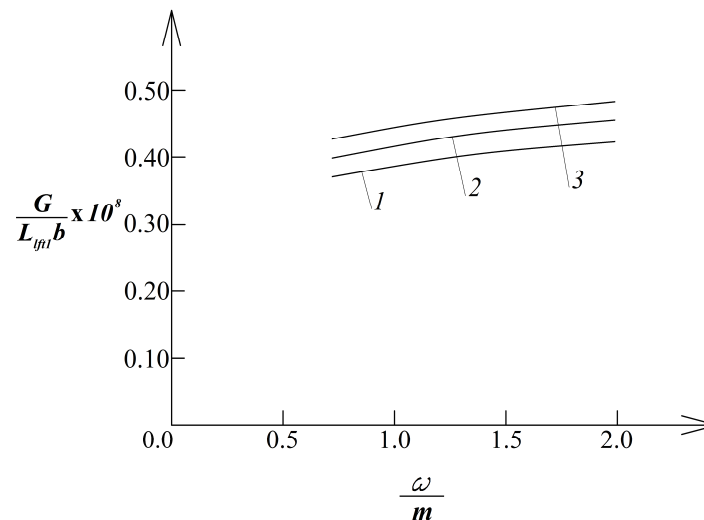


Fig. 14. The normalized SERR versus ω / m ratio for $q_1 / q_2 = 0.5$ (curve 1), $q_1 / q_2 = 1.0$ (curve 2) and $q_1 / q_2 = 2.0$ (curve 3).



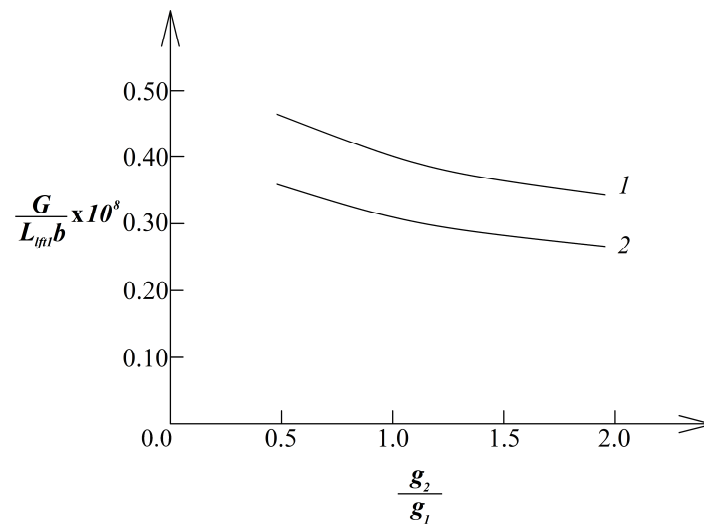


Fig. 15. The normalized SERR versus g_2 / g_1 ratio for the U-shaped structural member supported with a rotational spring in section, B_3 , (curve 1) and the U-shaped structural member supported with rotational springs in sections, B_3 and B_4 (curve 2).

The effect of variation of ω / m and q_1 / q_2 ratios on the normalized SERR in the U-shaped structural member supported with two rotational springs is explored too. This effect is illustrated by the plots displayed in Fig. 14.

Figure 15 displays the normalized SERR versus g_2 / g_1 ratio for the U-shaped structural member supported with rotational spring in section, B_3 , (curve 1) and supported with rotational springs in sections, B_3 and B_4 (curve 2).

It can be seen in Fig. 15 that the normalized SERR in the U-shaped structural member supported with rotational springs in sections, B_3 and B_4 , is lower compared to the U-shaped structural member supported with rotational spring in section, B_3 , only.

4. Conclusion

The preceding theoretical analysis is concerned with delamination of U-shaped functionally graded multilayered viscoelastic structural members supported by rotational springs. The springs have non-linear elastic behaviour (thus, the relationship between the restoring couple in the spring and the angle of rotation is non-linear). The left-hand vertical part of the structure is clamped in its lower end. The U-shaped structural members considered here are delaminated in their right-hand vertical part. The lower end of the right-hand delamination arm is under angle of rotation varying continuously with time. First, a U-shaped member supported by one rotational spring is analyzed. An approach for deriving solution of the SERR is presented. The method of the integral J is applied for performing a check-up of the solution obtained. The solution predicts that the SERR reduces when L_{fft1} / L_{fft1} ratio rises. Reduction of the SERR is predicted also in cases when n_1 increases. The increase of the number of layers, n , also results in a reduction of the SERR. It is found that growth of the values of parameters, g_1 , w_1 , r_1 , also induces reduction of the SERR. The effect of the structural member geometry (the latter is presented by a/l , h/l , R_1/l and h/b ratios) is also investigated. It is detected that the SERR rises with rise of a/l , h/l and R_1/l ratios. Rise of h/b ratio generates a reduction of the SERR. Concerning the effects of the parameters of the rotational spring support, it is predicted that the SERR reduces when the spring stiffness, ρ , grows. The growth of another parameter of the spring, m , causes rise of the SERR. Analysis of a U-shaped structural member supported by two rotational springs also is carried-out. The analysis predicts that the SERR reduces when ν / ρ and L_{fft2} / L_{fft1} ratios grow. The rise of ω / m and q_1 / q_2 ratios generate rise of the SERR. It is found also that the SERR in the U-shaped structural member supported by two rotational spring supports is lower compared to that in the U-shaped structural member with one rotational spring support. The knowledge obtained in the present paper can be applied in engineering practice for design of U-shaped structural members with considering the delamination behaviour. For example, it is possible to determine the desired stiffness of the rotational spring support in order to prevent delamination growth. For this purpose, the SERR has to be obtained at different stiffness of the rotational spring support by using the solution described in the present paper. The stiffness at which the SERR becomes equal to the delamination fracture toughness is the desired one. The thickness of the U-shaped structure can be determined in a similar way, i.e., calculations of the SERR have to be performed at different thicknesses (the thickness at which the SERR reaches the delamination fracture toughness is the desired one). Other parameters of the U-shaped structural member which are of critical interest for the engineering design like number and location of the rotational spring supports, number of layers in the structure, etc. can be determined in the same manner. It should be emphasized that the approach presented in this paper can be developed to analyze delamination in functionally graded multilayered viscoelastic structures with more complex geometry supported by rotational spring supports having non-linear elastic behaviour. For instance, delamination in engineering structures representing combinations of rectilinear members (like beams and columns) and curvilinear members like various arches and circular members can be treated by the present approach.

Author Contributions

V. Rizov is the only author of this article.

Acknowledgments

Not applicable.

Conflict of Interest

The author declared no potential conflicts of interest with respect to the research, authorship, and publication of this article.



Funding

The author received no financial support for the research, authorship, and publication of this article.


Data Availability Statements

The datasets generated and/or analyzed during the current study are available from the corresponding author on reasonable request.

References

- [1] Rzhantsyn, A.R., *Built-up Bars and Plates*, Stroyizdat, 1986.
- [2] Finot, M., Suresh, S., Small and large deformation of thick and thin-film multilayers: effect of layer geometry and compositional gradients, *Journal of the Mechanics and Physics of Solids*, 44, 1996, 683-721.
- [3] Kim, J.S., Paik, K.W., Oh, S.H., The Multilayer-Modified Stoney's Formula for Laminated Polymer Composites on a Silicon Substrate, *Journal of Applied Physics*, 86, 1999, 5474-5479.
- [4] Butcher, R.J., Rousseau, C.E., Tippur, H.V., A functionally graded particulate composite: Measurements and Failure Analysis, *Acta Materialia*, 47(2), 1999, 259-268.
- [5] Hirai, T., Chen, L., Recent and prospective development of functionally graded materials in Japan, *Materials Science Forum*, 308-311, 1999, 509-514.
- [6] Miyamoto, Y., Kaysser, W.A., Rabin, B.H., Kawasaki, A., Ford, R.G., *Functionally Graded Materials: Design, Processing and Applications*, Kluwer Academic Publishers, Dordrecht/London/Boston, 1999.
- [7] Han, X., Xu, Y.G., Lam, K.Y., Material characterization of functionally graded material by means of elastic waves and a progressive-learning neural network, *Composites Science and Technology*, 61(10), 2001, 1401-1411.
- [8] Long, V.T., Tung, H.V., Thermo-torsional buckling and postbuckling of thin FGM cylindrical shells with porosities and tangentially restrained edges, *Mechanics Based Design of Structures and Machines*, 51(12), 2023, 7056-7075.
- [9] Van Thinh, N., Van Tung, H., Free Vibration and Dynamical Analyses of FGM Plates with Porosity and Tangential Edge Constraints, *Journal of Vibration Engineering & Technologies*, 2023, DOI: 10.1007/s42417-023-01205-y.
- [10] Van Thinh, N., Van Tung, H., Nonlinear vibration of geometrically imperfect CNT-reinforced composite cylindrical panels exposed to thermal environments with elastically restrained edges, *Acta Mechanica*, 253(9), 2024, 1147-1164.
- [11] Gasik, M.M., Functionally graded materials: bulk processing techniques, *International Journal of Materials and Product Technology*, 39(1-2), 2010, 20-29.
- [12] Nemat-Allal, M.M., Ata, M.H., Bayoumi, M.R., Khair-Eldeen, W., Powder metallurgical fabrication and microstructural investigations of Aluminum/Steel functionally graded material, *Materials Sciences and Applications*, 2(5), 2011, 1708-1718.
- [13] Shrikantha Rao, S., Gangadharan, K.V., Functionally graded composite materials: an overview, *Procedia Materials Science*, 5(1), 2014, 1291-1299.
- [14] Wu, X.L., Jiang, P., Chen, L., Zhang, J.F., Yuan, F.P., Zhu, Y.T., Synergetic strengthening by gradient structure, *Materials Research Letters*, 2(1), 2014, 185-191.
- [15] Arefi, M., Rahimi, G.H., Non-linear analysis of a functionally graded beam with variable thickness, *Scientific Research and Essays*, 8(6), 2013, 256-264.
- [16] Arefi, M., Nonlinear analysis of a functionally graded beam resting on the elastic nonlinear foundation, *Journal of Theoretical and Applied Mechanics*, 44(2), 2014, 71-82.
- [17] Arefi, M., Elastic solution of a curved beam made of functionally graded materials with different cross section, *Steel and Composite Structures*, 18(3), 2015, 659-672.
- [18] Saiyathibrahim, A., Subramaniyan, R. Dhanapl, P., Centrifugally cast functionally graded materials – review, In: *International Conference on Systems, Science, Control, Communications, Engineering and Technology*, 2016.
- [19] Mahamood, R.M., Akinlabi, E.T., *Functionally Graded Materials*, Springer, 2017.
- [20] Rizov, V., Effects of Periodic Loading on Longitudinal Fracture in Viscoelastic Functionally Graded Beam Structures, *Journal of Applied and Computational Mechanics*, 8(1), 2022, 370-378.
- [21] Hutchinson, J.W., Suo, Z., Mixed mode cracking in layered materials, *Advances in Applied Mechanics*, 64, 1992, 804 - 810.
- [22] Dolgov, N.A., Effect of the elastic modulus of a coating on the serviceability of the substrate-coating system, *Strength of Materials*, 37(2), 2002, 422-431.
- [23] Dolgov, N.A., Determination of Stresses in a Two-Layer Coating, *Strength of Materials*, 37(2), 2005, 422-431.
- [24] Dolgov, N.A., Analytical Methods to Determine the Stress State in the Substrate-Coating System Under Mechanical Loads, *Strength of Materials*, 48(1), 2016, 658-667.
- [25] Dowling, N., *Mechanical Behavior of Materials*, Pearson, 2007.
- [26] Khot, U.M., Gaonkar, A.K., Effect of Axial Load on Static and Eigenvalue Characteristics of MEMS with Compliant Support, 68th Congress of the Indian Society of Theoretical and Applied Mechanics (ISTAM), 2023.
- [27] Nuguzhinov, Zh.S., Akhmediev, S.K., Zholmagambetov, S.R., Khabidolda, O., Calculation of continuous beams taking into account the elastic compliance of supports, *Bulletin of Karaganda University*, 4(92), 2018, 139-147.
- [28] Korenev, B.G., Reznikov, L.M., *Dynamic absorbers of vibrations. Theory and technical applications*, Nauka, 1988.
- [29] Tsankov, T., *Theory of Plasticity*, Science, 1996.
- [30] Rizov, V.I., Analysis of the Strain Energy Release Rate for a Delamination Crack in a Multilayered Beam with Material Non-Linearity, *IOP Conference Series: Materials Science and Engineering*, 473, 2019, 012002.
- [31] Broek, D., *Elementary Engineering Fracture Mechanics*, Springer, Netherlands, 1982.

ORCID iD

Victor Rizov  <https://orcid.org/0000-0002-0259-3984>



© 2024 Shahid Chamran University of Ahvaz, Ahvaz, Iran. This article is an open access article distributed under the terms and conditions of the Creative Commons Attribution-NonCommercial 4.0 International (CC BY-NC 4.0 license) (<http://creativecommons.org/licenses/by-nc/4.0/>).

How to cite this article: Rizov V. The Effect of Delamination Between Layers in U-shaped Members Made of Functionally Graded Multilayered Viscoelastic Materials, *J. Appl. Comput. Mech.*, xx(x), 2024, 1-12. <https://doi.org/10.22055/jacm.2024.46014.4449>

Publisher's Note Shahid Chamran University of Ahvaz remains neutral with regard to jurisdictional claims in published maps and institutional affiliations.

